ACS Photonics

Article

pubs.acs.org/journal/apchd5

Toward Label-Free Super-Resolution Microscopy

W. Ruchira Silva, Christian T. Graefe, and Renee R. Frontiera*

Department of Chemistry, University of Minnesota Minneapolis, Minnesota 55455, United States

Supporting Information

ABSTRACT: We propose and implement a far-field spectroscopic system for imaging below the diffraction limit without the need for fluorescence labeling. Our technique combines concepts from Stimulated Emission Depletion (STED) microscopy and Femtosecond Stimulated Raman Spectroscopy (FSRS). The FSRS process generates signal through the creation of vibrational coherences, and here we use a toroidal-shaped decoherence pulse to eliminate vibrational signal from the edges of the focal spot. The nonlinear dependence on decoherence pulse power enables subdiffraction imaging. As in STED, the resolution is in theory infinitely small given infinite decoherence pulse power. Here, we first experimentally demonstrate that the photophysical principles behind our super-resolution Raman imaging method are sound. We then prove that addition of the decoherence pulse significantly improves the spatial resolution of our microscope, achieving values beyond the diffraction limit. We discuss future directions for this technique, including methods to reach resolution on the order of ten nanometers.

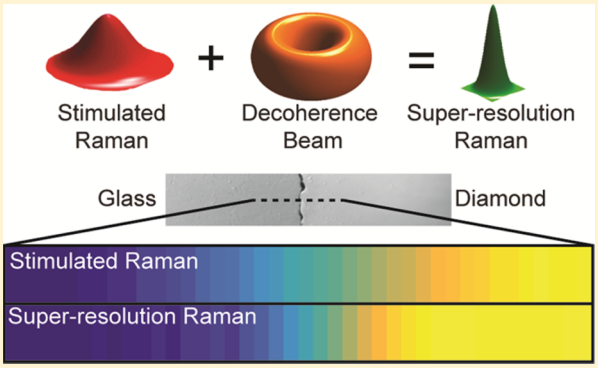

KEYWORDS: *Raman imaging, subdiffraction imaging, label-free, super-resolution*

Imaging of soft matter on nanometer length scales is of crucial importance. In fields as diverse as molecular biology, materials science, and bioengineering, changes in chemical composition on nano- and meso- length scales play a large role in understanding structure and function. For example, in cellular membranes, individual membrane proteins have sizes well below the diffraction limit and exist in very heterogeneous environments. In many cases it is unclear how these environmental heterogeneities affect function. Imaging methods which provide label-free approaches to obtaining dynamic information regarding chemical conformation on these length scales would be valuable in understanding cellular signaling and transport properties. However, it is challenging to use optical methods on these length scales due to the optical diffraction limit.

Super-resolution microscopy has revolutionized imaging by breaking the traditional far-field diffraction limit. Rather than the ~250 nm Abbe limit of resolution for optical microscopy, fluorescence-based super-resolution imaging now routinely achieves resolution on length scales less than 10 nm. The development of techniques such as stimulated emission depletion (STED),[1] photoactivated localization microscopy (PALM),[2] and stochastic optical reconstruction microscopy (STORM),[3] have transformed microscopy by enabling rapid acquisition of images with breath-taking nanometer resolution. These extraordinary techniques were recently recognized with the 2014 Nobel Prize in Chemistry.

Despite the tremendous successes and scientific advances enabled by these novel techniques, current super-resolution microscopies require external labeling with photoswitchable fluorophores. Fluorophore labeling necessitates significant sample preparation and can be experimentally challenging. Fluorophores may quench, leading to a sudden loss of signal. With sizes on molecular or protein length scales, the labels have the possibility of perturbing the structure or dynamics under investigation.[4] Additionally, it can be challenging to label multiple components simultaneously, and multicolor super-resolution imaging methods will likely be limited to tracking at most dozens of concurrently labeled molecular species. Despite significant advances in developing photoswitchable fluorophores optimized for super-resolution imaging, other optical techniques may obviate the need for labeling.

Raman spectroscopy provides a convenient, nondestructive method for chemical identification without the need for external labels. The relatively weak Raman scattering processes may be enhanced significantly through the use of stimulated and resonance Raman spectroscopies. Microscopies based on stimulated Raman spectroscopy (SRS) and coherent anti-Stokes Raman spectroscopy (CARS) have enabled significant new biological discoveries.[5−10] As a vibrationally sensitive technique, a key advantage of Raman spectroscopy is the ability to identify a number of unique chemicals or functional groups within a given sample spot. For example, in a cellular system, Raman microscopy is easily able to quantify lipid, protein, and water content in a given focal volume.[8] As stimulated Raman techniques use four-wave mixing to coherently generate a signal, they are relatively free from background fluorescence.[11]

Received: August 20, 2015
Published: December 28, 2015

DOI: 10.1021/acsphotonics.5b00467
ACS Photonics 2016, 3, 79−86

Additionally, the coherent nature of the signal means all Raman photons can be easily collected, as opposed to spontaneous Raman spectroscopy.

Far-field diffraction-limited Raman imaging is finding tremendous applications in biomedical fields, including the demonstration of video-frame rate imaging.[8] Currently, most Raman microscopies are limited in spatial resolution by the optical diffraction limit. Surface- and tip-enhanced Raman spectroscopies can provide subdiffraction resolution but have difficulty providing quantitative information, and the plasmonic materials needed may affect reaction dynamics or cause sample degradation.[12,13] A far-field Raman microscope with resolution well below the diffraction limit would be valuable in the ability to image structure and dynamics in soft matter samples, such as cellular membranes or polymeric photovoltaics. Recent far-field work in this area has included calculations and measurements determining that the resolution in a CARS microscope can be improved by 1.5 times through point spread function engineering.[14] Subsequent implementation by Kim et al. achieved a deconvolved resolution of 130 nm with near-infrared light.[15] These uses of Toraldo-style pupil phase filtering to reduce the size of the effective point spread function enhances the resolution to a value more than two times the diffraction limit, with the ultimate resolution likely limited by the effects of side lobes in the spatial profile.

Other recent methods to achieve subdiffraction imaging without using fluorescent labels have utilized switching of optical absorption or modulation of photothermal effects. Wang et al. were able to image nonfluorescent species below the diffraction limit using saturable absorption in conjunction with concepts from STED, achieving resolution of 225 nm with near-infrared light.[16] Tzang et al. used the effects of photothermal gradients on Raman lineshapes in order to improve spatial resolution, enhancing the resolution in one paper from 650 nm down to 440 nm,[17] and in another down to 105 nm.[18] These studies prove that concepts from the fluorescence-based super-resolution imaging techniques can be applied to other imaging modalities such as absorption or Raman. For widespread application, desirable features include label-free chemical specificity, as well as the ability to achieve resolution on the critical sub-50 nm length scale using visible or near-infrared light.

Here we propose and implement another method for subdiffraction Raman imaging. This technique is based on the photoswitching principle of STED, combined with a stimulated Raman technique known as femtosecond stimulated Raman spectroscopy (FSRS).[19] We show that the combination of these techniques results in imaging with resolution below that allowed by the numerical aperture of the objective used. This technique has the potential to achieve resolution such as the <50 nm resolution routinely obtained with STED. We believe these results represent a new approach toward far-field super-resolution Raman microscopy, and provide a route toward label-free optical imaging on the 10 nm length scale.

RESULTS AND DISCUSSION

Our subdiffraction Raman imaging technique is based on a combination of STED imaging and FSRS. STED is a fluorescence-based super-resolution technique which relies on spatial light shaping and the nonlinear stimulated emission response of fluorophores.[20] In STED, a Gaussian beam photoexcites a labeled sample, and a doughnut-shaped beam stimulates the emission in the outer edges of the photoexcited region. Thus, fluorescence is emitted only from the center of doughnut, which can routinely attain spatial resolution less than 50 nm in the x and y directions under appropriate powers and focusing conditions.[21] The key photophysical principle needed to achieve super-resolution is to ensure that the signal is "turned off" by the addition of a spatially shaped laser pulse and that this signal reduction is nonlinear with power.

FSRS is a stimulated Raman technique that provides a broadband Raman spectrum in as few as two laser pulses (i.e., in 2 ms with a kHz laser source).[19] The technique uses a picosecond Raman pump pulse in conjunction with a femtosecond probe pulse to generate a coherent Raman signal.[22] A FSR spectrum is reported as Raman gain, which is the ratio of the Raman pump-on spectrum divided by the Raman pump-off spectrum. In FSRS, vibrational coherences are generated through interactions with the pump and probe pulses. These coherences typically persist for 10^2 to 10^3 femtoseconds, depending on the vibrational dephasing time of the mode of interest. At some point during this dephasing time, there is a third interaction with the pump field, which leads to the generation of the Raman signal. Thus, FSRS is a nonlinear four-wave mixing technique utilizing vibrational coherences to generate stimulated Raman signals. FSRS has previously been utilized for diffraction-limited imaging.[23] We utilize this concept for subdiffraction Raman by using a third beam to destroy the vibrational coherence in a spatially defined area, similar to the stimulated emission beam used in STED.

Figure 1 provides a conceptual illustration of our super-resolution Raman imaging technique. Two beams with

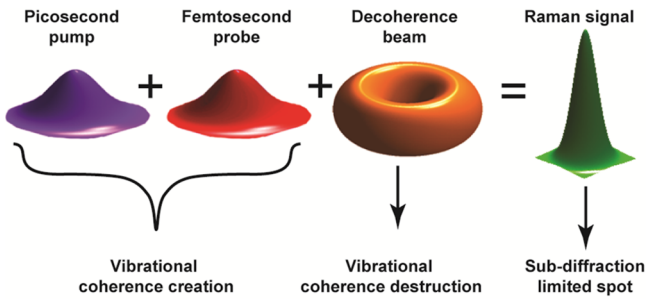

Figure 1. Schematic depiction of subdiffraction Raman imaging. Two pulses, a picosecond pump and femtosecond probe, interact to create vibrational coherences in the sample. A spatially shaped decoherence beam destroys the vibrational coherences in the ring region, leaving coherence and subsequent stimulated Raman signal generation in the center region.

Gaussian spatial profiles, termed the Raman pump and probe beams, interact in the sample to create vibrational coherences in all Raman active modes. With no additional beams, this setup is similar to that of a diffraction-limited femtosecond stimulated Raman microscope.[23] In subdiffraction Raman, we add an additional doughnut-shaped pulse, termed the decoherence pulse, which interacts with the sample and destroys the vibrational coherence. This decoherence pulse is spatially shaped by a 2π helical phase plate, generating a beam with one central node. The coherence destruction prevents femtosecond stimulated Raman signal generation in the ring region by driving an alternative four-wave mixing pathway.[24] The vibrational coherence only survives in the center of the doughnut, and femtosecond stimulated Raman signal is only generated in this region. Just as in STED, the coherence

DOI: 10.1021/acsphotonics.5b00467
ACS Photonics 2016, 3, 79−86

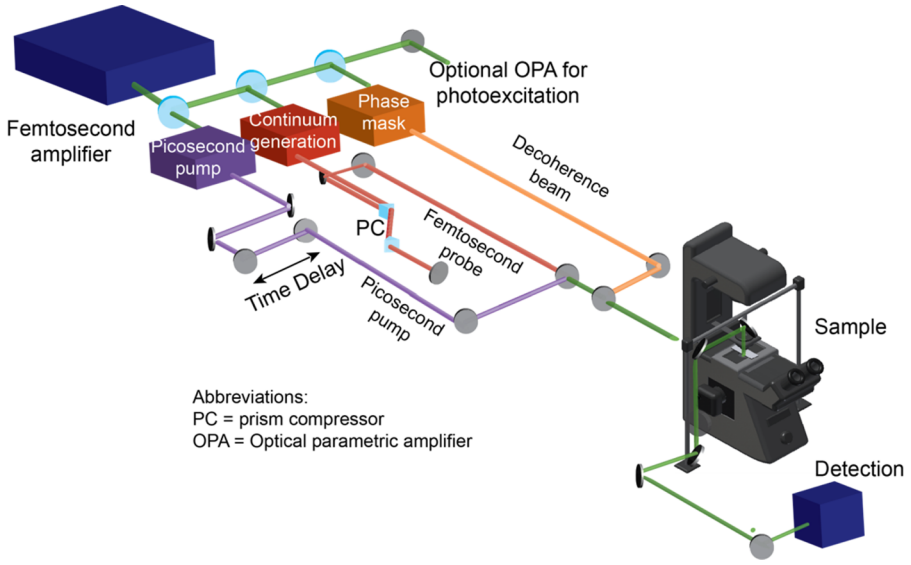

Figure 2. Experimental setup for super-resolution Raman imaging. Subdiffraction Raman microscopy is enabled by the generation of three pulse trains from a single femtosecond amplifier. The pulses are overlapped at the sample, and subdiffraction Raman signal is detected in a transmission geometry.

destruction must be nonlinear in order to achieve subdiffraction resolution. This method provides a unique way to "turn off" the femtosecond stimulated Raman signal by the addition of a laser pulse. As the principles are similar to STED, the resolution is in theory infinitely small given an infinite decoherence pulse power.

Figure 2 shows the experimental depiction of a system constructed to test the photophysical principles of the technique. Details are provided in the Methods section. These proof-of-principle measurements utilize a kHz femtosecond amplifier and CCD detector, although alternative light and detection sources are discussed below. The amplifier output is split into the three beams necessary for super-resolution Raman imaging: the picosecond Raman pump pulse, the broadband femtosecond probe pulse, and the spatially shaped decoherence pulse. These beams are focused onto the sample with an inverted microscope, and signal is collected in transmission mode with a condenser utilized for collimation. For the measurements described here, the pump and decoherence beams are centered at 800 nm, and the probe beam is a near-infrared continuum extending from 830−1000 nm. The cross correlation between the femtosecond probe and decoherence beams with the lens geometry was measured to be 140 ± 30 fs, as determined by the optical Kerr effect in a 2 mm cuvette of cyclohexane.

Our initial experiments demonstrate the feasibility of turning off the femtosecond stimulated Raman signal through the addition of a decoherence pulse. In Figure 3A, we show the photoswitching in cyclohexane, which was taken with Gaussian spatial profiles for all three beams. Without the decoherence pulse, the cyclohexane Raman gain is 13.1. Upon addition of the decoherence pulse, the signal drops to 0.4, a 97% reduction in Raman signal. It is clear that the decoherence pulse is interrupting the FSRS signal generation pathway by promoting another four-wave mixing process which is not detected. In these measurements, the Raman pump pulse was held constant at a power of 8.8 W/cm^2, which is similar to the 20 W/cm^2 reported for Raman imaging measurements on living mice.[6,8]

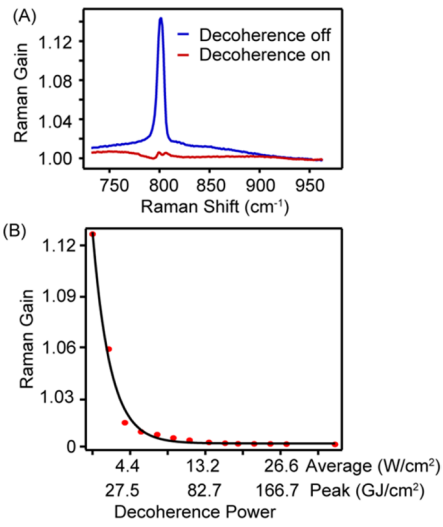

Figure 3. (A) Photoswitching of the cyclohexane Raman gain signal upon additional of the decoherence pulse, using beams with Gaussian spatial profiles. Measurements were taken with an 800 nm, 8.8 W/cm^2 Raman pump pulse and 800 nm, 22 W/cm^2 decoherence pulse. We see nearly 100% switching, indicating near complete destruction of the femtosecond stimulated Raman signal. (B) Raman gain signal as a function of decoherence beam power. The acquisition time per point was six seconds for panels A and B.

The STED technique is able to achieve subdiffraction imaging due to the nonlinear dependence of fluorescence quenching. As the spatial profile of the doughnut beam varies on the length scale of the wavelength of light, nonlinear dependence is needed. Effectively, this means that even the weak fields near the center of the doughnut beam have sufficient intensity to quench the fluorescence. As there is a node at the center of the doughnut beam, there is no quenching in this region. For super-resolution Raman to achieve subdiffraction limits, a similar intensity dependence is required. In Figure 3B, we show the nonlinear power dependence of the Raman gain amplitude, as a function of both the average power and the peak power of the decoherence beam. As the power of

DOI: 10.1021/acsphotonics.5b00467
ACS Photonics 2016, 3, 79−86

the decoherence beam is increased, we initially see an exponential drop in the Raman signal magnitude, up to average powers on the order of 10 W/cm^2. Past this threshold, we see saturation of the transition, and the Raman signal remains near zero for all powers measured. An average power of 10 W/cm^2 corresponds to a decoherence beam peak power of 62 GJ/cm^2. This power is comparable to the peak powers used in STED, which are typically in the range of 16 GJ/cm^2 to 21 TJ/cm^2.[25−27] This nonlinear dependence is ideal for subdiffraction Raman imaging and enables efficient photoswitching behavior at length scales better than the diffraction limit.

Other factors, which affect the decoherence efficiency and, thus, will impact the attainable resolution, are the polarization of the decoherence beam relative to the stimulated Raman beams, and the time-delay dependence of the decoherence beam relative to the Raman pump−probe temporal overlap. These parameters can be easily controlled to routinely achieve maximum photoswitching of the FSRS signal. Optimization of decoherence is necessary for achieving the maximum improvement in spatial resolution.

Figure 4A shows the effect of decoherence beam polarization on the Raman photoswitching efficiency for the ring breathing

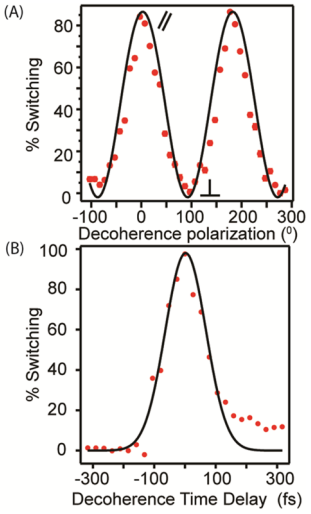

Figure 4. Photophysical optimization of the super-resolution Raman decoherence process using all three beams with Gaussian spatial profiles. (A) Polarization dependence of photoswitching in super-resolution Raman. As expected, maximal photoswitching occurs when the decoherence beam has polarization parallel to the Raman pump and probe beams. (B) Dependence of decoherence pulse temporal overlap on photoswitching. Negative time delays indicate points when the temporal peak of the decoherence pulse precedes the Raman pump and probe maxima. Data in both figures were taken with an 800 nm, 8.8 W/cm^2 Raman pump pulse, an 800 nm, 22.0 W/cm^2 decoherence pulse, and a six second acquisition time per point.

mode of cyclohexane. Here we define photoswitching as the percent of Raman gain signal lost upon addition of the decoherence pulse, in which 100% photoswitching would represent complete loss of signal. In Figure 4, spectra were taken using all three beams with Gaussian profiles. In these measurements, it is important to realize that the phase plate does not affect the polarization of the decoherence beam, as the polarization is defined by the input beam polarization. We see that the photoswitching efficiency is maximized when all beams have the same polarization, indicated at 180° intervals of decoherence beam polarization. As the polarization is rotated, the photoswitching efficiency decreases, due to inefficient destruction of the Raman vibrational coherence.

Varying the time delay of the decoherence pulse dramatically affects the photoswitching efficiency, as shown in Figure 4B. When the decoherence beam precedes the creation of the vibrational coherence, indicated by negative delays, there is no destruction of the coherence, as expected. Maximum coherence destruction occurs at or very close to the time point of maximum overlap. There is some photoswitching at later time delays, likely due to the interaction of the decoherence pulse with the long-lived vibrational coherence. The full width at half-maximum of the primary peak in Figure 4B is 150 ± 10 fs, which is similar to the cross-correlation value of 140 ± 30 fs between the decoherence beam and femtosecond Raman probe beam. This indicates that disruption of the FSRS four-wave mixing pathway is most effective when all three beams are interacting with the sample.

Following these proof-of-concept measurements of the photoswitching characteristics of stimulated Raman spectroscopy, we demonstrate in Figure 5 that the addition of the decoherence pulse significantly improves the resolution of our stimulated Raman imaging system. Figure 5b shows an optical image of a piece of 40 μm thick CVD diamond used for imaging. Rather than determining resolution by imaging two

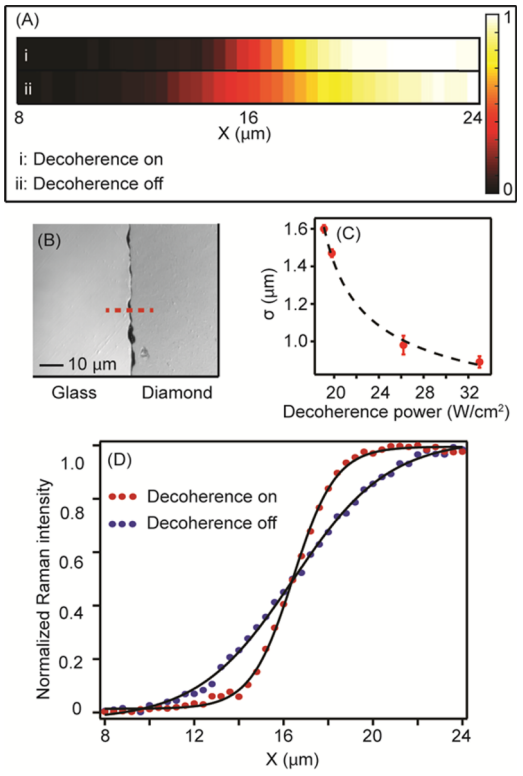

Figure 5. Raman imaging across a diamond plate edge. (A) Normalized Raman intensity as a function of position, with decoherence beam on and off. (B) Optical microscope image of diamond plate. (C) Spatial resolution improvement, represented as the fitted value from a sigmoidal curve, as a function of decoherence beam power. (D) Line scan across diamond plate, showing clear improvement of resolution with the addition of the decoherence beam. Parts A and D were taken with a 800 nm Raman pump pulse with a power of 13.1 W/cm^2, an 800 nm decoherence beam with power of 33 W/cm^2, and a 2 s acquisition time per point. A 20× objective with a numerical aperture of 0.40 was used for these scans.

DOI: 10.1021/acsphotonics.5b00467
ACS Photonics 2016, 3, 79−86

closely spaced objects, imaging over the interface of a single sharp object can provide an accurate measure of the resolution of any microscope by using the rate parameter from a sigmoidal fit.[28] This approach avoids any need to deconvolute with the sample thickness profile, such as with polystyrene beads with high curvature. To determine the resolution, we fit the Raman intensity as a function of position to eq 1:

$$y = \frac{A}{1 + e^{(x_0 - x)/\sigma}} \quad (1)$$

The fitted value σ is then multiplied by a factor of 3.33 to define the resolution of the system. This assumes that the object has a perfectly sharp edge. If this assumption is not accurate, the extracted value can be considered an upper bound for resolution in the microscope.

In Figure 5A,D, we show the Raman intensity of the 1332 cm^{-1} C−C stretching mode of diamond as a function of position, as the sample is translated through the focal volume. These spectra were taken with a 20× objective with a numerical aperture of 0.40. The blue trace in Figure 5d shows the Raman intensity when the decoherence beam is off. When we assume that the diamond plate has a perfectly sharp edge, the resolution of the system is 5.07 ± 0.17 μm. This is above the diffraction limit, both due to the 40 μm sample thickness as well as because both Raman pump and probe beams are not perfectly backfilling the objective, as is common in imaging experiments.[29] When the decoherence beam is turned on and the same sample is scanned, there is a dramatic improvement in resolution. The line scan can be fit to give a resolution value of 2.96 ± 0.10 μm, which is close to a factor of 2 in improved resolution. These spectra were taken with a Raman pump power of 13.1 W/cm^2, similar to the 20 W/cm^2 previously used for CARS and SRS imaging of living mice.[6,8] Photodegradation is possible in some samples at these powers but was not observed in these experiments.

Just as in STED, in our Raman imaging process we would expect the resolution to improve as the decoherence beam power is increased. In Figure 5c, we show the dependence of the sigmoidal value as a function of power, as we scan across the same diamond interface. The point corresponding to 33 W/cm^2 is the data shown in Figures 5A,D. Over the range of powers accessible to our laser and detection system, we see significant improvement in resolution as the power increases from 20 to 33 W/cm^2. This behavior is similar to that observed in STED as the stimulated emission power is increased.[20]

Imaging with several experimental configurations shows definitive resolution below the Abbe diffraction limit with the addition of the decoherence beam. Figure S1 shows the scans representative of resolution limits readily achievable with 10× and 20× microscope objectives and a 10 μm thick piece of CVD diamond. These low numerical aperture objectives were chosen to make best use of the low repetition rate, high peak power laser utilized in these studies. By decreasing the thickness of the diamond as compared to that used for imaging results shown in Figure 5, we are better able to characterize the current spatial resolution of the technique. In both cases, the resolution improves by nearly 40% upon addition of the decoherence beam. For the 20× objective, sigmoidal rate fitting as described above gives a resolution of 1.53 ± 0.07 μm with the decoherence beam off, and resolution of 0.93 ± 0.03 μm with the decoherence beam on. The Abbe diffraction limit should be 1.37 μm for this system, which is 47% higher than the resolution value of 0.93 μm reached in this experiment. For the 10× objective, similar analysis shows that the diffraction limit is 6% higher than the value achieved with the decoherence beam on.

The performance of our Raman imaging system in two dimensions is shown in Figure 6. We took line scans across the

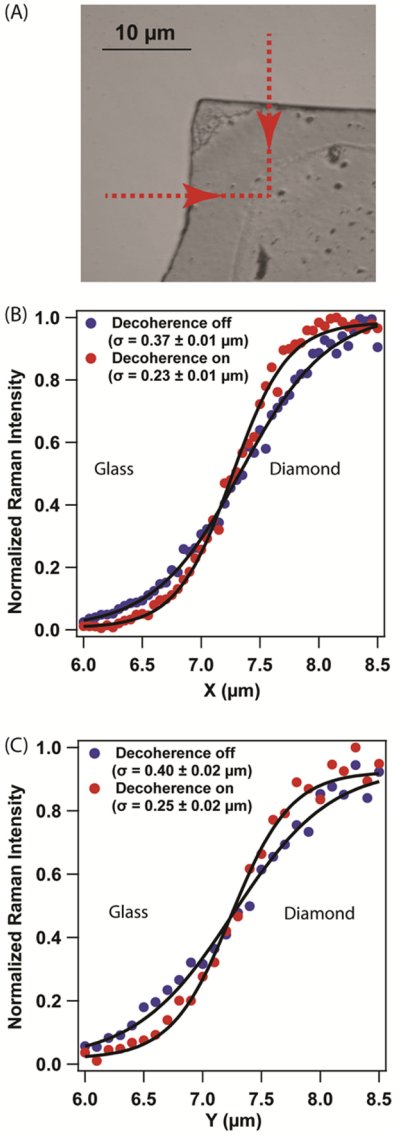

Figure 6. Resolution increase in two dimensions with subdiffraction Raman imaging. (A) The optical image of a corner of a diamond plate used for image. (B) Resolution improvement with the 800 nm decoherence pulse on across the *X* axis. (C) Resolution improvement with the 800 nm decoherence pulse on across the *Y* axis. The acquisition time was 2 s per spectrum, and scans were taken with a 20× objective with a numerical aperture of 0.40. The 800 nm Raman pump power was 13.1 W/cm^2 and the decoherence power was 26.2 W/cm^2.

X and *Y* axes of a corner of a diamond plate, which is shown in the optical image shown in Figure 6A. In parts B and C are the line scans corresponding to the *X* and *Y* dimensions, respectively. The resolution values for these scans with the decoherence beam off are 1.35 ± 0.06 μm for the *X* dimension and 1.24 ± 0.04 μm for the *Y* dimension. The values with the decoherence beam off are just slightly below the diffraction limit for this system, as allowed for a coherent stimulated

DOI: 10.1021/acsphotonics.5b00467
ACS Photonics 2016, 3, 79−86

Raman process. When the decoherence beam is on, the sigmoidal constants drop to 0.82 ± 0.05 μm for the X dimension and 0.78 ± 0.03 μm for the Y dimension. Within error, these values are quite similar, and indicate nearly symmetric subdiffraction performance of our decoherence beam. Deviation from symmetric performance could arise from the nonrectilinear interface of the diamond plate, or from imperfect overlap of the decoherence beam with the Raman pump and probe beams.

As stimulated Raman is a coherent nonlinear process, it is not suitable to use the Abbe diffraction limit to define spatial resolution.[30] Analysis of signal generation in CARS has demonstrated that the coherent nature of the process can "scramble the spatial resolution",[31] and determining the resolution limit requires careful consideration of the signal buildup and propagation for each sample.[32] Previous experiments have shown improvements over the diffraction limit, reaching resolution as low as 300 nm using high numerical aperture objectives.[33,34] However, most stimulated Raman microscopes operate well above these limits of resolution.[35] The varying spatial profile of the round polystyrene beads typically used for resolution measurements, when convoluted with the CARS signal generation process, may also impact the observed resolution. Thus, we believe our improvement in imaging resolution through the use of a doughnut-shaped decoherence beam represents a novel approach to imaging beyond the diffraction limit. However, in future measurements designed to improve the spatial resolution of our technique, issues with polarization effects and electric field distortion with the use of high numerical objectives will likely be significant. High numerical objective optics were not used in this work due to photodegradation issues with the high peak powers of the kHz laser, but potential issues with field distortion must first be overcome in order for the technique to achieve widespread use and applicability. The precedent of high resolution phase-matched SRS microscopy, as well as the development of high NA polarization-maintaining objectives, is encouraging in this regard.

The increase in imaging resolution we observe solely upon addition of the decoherence laser beam provides solid evidence that the photophysical principles behind our super-resolution Raman technique will enable significant resolution improvements in label-free imaging. We have clearly demonstrated that far-field subdiffraction Raman imaging is feasible with these methods. The key to this novel technique is the combination of FSRS with STED. In the region illuminated by the doughnut-shaped pulse, we promote a four-wave mixing pathway which does not result in the generation of a Stokes-shifted Raman signal. Likely, this pathway is a coherent anti-Stokes Raman spectroscopy pathway, in which the decoherence beam acts as the third field interaction to promote the generation of an anti-Stokes signal. This pathway results in a signal with a different phase vector and different frequency than the desired FSRS signal and, thus, is not detected. In the central region, there is no field intensity from the decoherence pulse, and the FSRS pathway proceeds as usual. Figure S4 shows an increase in detected photons on the anti-Stokes side of the spectrum, which is present only when all three beams are incident on the sample, consistent with this CARS hypothesis.

For this approach to achieve transformative improvements in label-free imaging resolution, higher spatial resolution is required. This will require changing our existing proof-of-concept system to one with different light and detection instrumentation. We estimate that through the use of a high repetition rate femtosecond amplifier and high modulation depth lock-in amplification, we should obtain pixel dwell times on the order of tens of seconds for samples with reasonable Raman cross sections. The Supporting Information details these estimates for specific light and detection sources, based on our work here and previously reported literature values for various instrumentation in stimulated Raman imaging.

Our unique approach to subdiffraction imaging has several potentially valuable advantages over current imaging technologies. First, the ability to obtain subdiffraction images without fluorophore labeling is significant. Our method is particularly attractive as it is theoretically possible to achieve unlimited spatial resolution, assuming infinite decoherence pulse power. Second, with Raman microscopy it is possible to identify the chemical composition of the sample, probing a variety of species simultaneously. By using femtosecond stimulated Raman microscopy, as opposed to picosecond stimulated Raman microscopy, we are able to obtain an entire vibrational spectrum in a single acquisition. The use of FSRS also provides for the possibility of monitoring femtosecond time scale dynamics on a subdiffraction length scale, with the addition of a femtosecond photoexcitation pulse. Finally, as our technique is based on scattering and not absorption, it should be less sensitive to photodegradation. We believe these capabilities will make subdiffraction Raman a valuable technique in a variety of fields. Our technique offers unique advantages over other far-field label-free super-resolution techniques, which include concepts such as phase-filtered four-wave mixing,[15] transient saturable absorption,[16] temperature modulation,[17] chemometric algorithms,[36] and theoretical proposals for super-resolution CARS.[37−39]

CONCLUSION

The work presented here conclusively demonstrates that the photophysical concepts behind the far-field subdiffraction Raman system proposed here are sound. The addition of a decoherence pulse interferes with the femtosecond stimulated Raman pathway, selectively turning off the signal in a spatially defined region. As the mechanism is similar to STED, resolution on the nanometer length scale should ultimately be achievable. Work is ongoing in the technological directions mentioned above, which will enable super-resolution imaging without the need for external fluorescent labels. This should lead to advances in soft matter imaging, including exciting developments in fields as diverse as health, biology, and materials science.

METHODS

Laser System. The FSR spectrometer has been described previously.[11] The same system was used for super-resolution imaging, with several modifications. The output of a 4.6 W, 90 fs, 800 nm, 1 kHz Ti:sapphire amplifier (Coherent Libra-F-1K-HE-110 with VitesseTM oscillator) was split into the three beams necessary for super-resolution imaging.

The Raman pump pulse is generated by sending 440 mW of the fundamental laser beam through a grating filter, to create a picosecond pulse of tunable pulse duration. The grating filter consists of a 100 mm cylindrical lens (Thorlabs), a 1200 gr/mm grating blazed at 750 nm (Edmund Optics), and an adjustable slit. The beam diameter is optimized with a 1:2 telescope, and the power is attenuated at the sample with a

DOI: 10.1021/acsphotonics.5b00467
ACS Photonics 2016, 3, 79−86

variable neutral density filter. For imaging experiments, we found that slightly modulating the time delay with a home-built vibrating speaker reduced background from cross phase modulation.

The broadband probe pulse was generated by focusing ∼1.5 mW of the fundamental beam into a 3 mm thick piece of sapphire (Newlight Photonics), generating a broadband continuum. The fundamental is partially filtered with a glass filter (Thorlabs RG830), and the beam is compressed with a pair of fused silica prisms (Thorlabs AFS-FS).

The decoherence beam was generated using a vortex phase plate (RPC Photonics, VPP-1a), with a 2π helical phase designed for a beam at 796.3 nm. The power of this beam was attenuated at the sample with a waveplate (Newport) and thin film polarizer (Thorlabs) and with a variable neutral density filter. The x and y positions and the rotation of the phase plate were controlled with manual stages. The time delay of the decoherence beam was controlled with a piezo actuator (Newport Picomotor Actuator Model 8302).

Experiments probing the fundamental nature of the decoherence photoswitching process were conducted without a microscope. In these experiments, the three beams were sent through a focusing lens (10 cm focal length, 2 in. diameter), and focused on a 1 or 2 mm cuvette with cyclohexane. The probe beam was sent through the center of the lens, and pump and decoherence beams were slightly noncollinear (∼1°) in the horizontal direction.

Imaging experiments were performed by sending the three beams through the back aperture of an inverted microscope (Olympus IX-73) and reflecting them upward to the sample with a silver mirror. Olympus infinity-corrected objectives (Plan 20X air, 0.4 NA; Plan 10X air, 0.25 NA) were used to focus all beams to the sample. A condenser (IX2-LWUCD, NA 0.55) was used to collect and collimate the probe beam and coherent stimulated Raman signal. The sample was translated with a 3D piezo scanning stage (MadCity Laboratories NanoLPQ) with subnanometer resolution.

The probe and signal were filtered (Thorlabs RG1000), sent into a spectrograph and dispersed by a 600 gr/mm grating blazed at 750 nm. The signals were focused onto a CCD array detector (Princeton Instruments 100F). Data collection at a triggered 1 kHz repetition rate was controlled by a home-written LabVIEW program. A chopper (Thorlabs MC2000) was used to alternate shots between Raman-pump-on and Raman-pump-off, and spectra are presented as Raman gain, thus, normalizing for relative probe intensity across the spectral region of interest. A home-built, flip-flop circuit controlled the triggering for the detector.

Samples. Neat cyclohexane was purchased from Sigma-Aldrich and used without further purification. The CVD diamond was purchased from Diamond Materials GMBH and samples were 10 or 40 μm thick. Defects in the diamond were minimal, as evidenced by the Raman spectral line width and lack of birefringence.

■ ASSOCIATED CONTENT

Supporting Information

The Supporting Information is available free of charge on the ACS Publications website at DOI: 10.1021/acsphotonics.5b00467.

Approaches to high-speed super-resolution Raman imaging, resolution limits under additional focusing conditions, axial resolution, biological compatibility, and CARS spectra (PDF).

■ AUTHOR INFORMATION

Corresponding Author

*E-mail: rrf@umn.edu. Tel.: 612-624-2501.

Notes

The authors declare no competing financial interest.

■ ACKNOWLEDGMENTS

We gratefully acknowledge University of Minnesota startup funding for support of this work.

■ REFERENCES

(1) Hell, S. W.; Wichmann, J. Breaking the Diffraction Resolution Limit by Stimulated Emission Depletion Fluorescence Microscopy. *Opt. Lett.* **1994**, *19*, 780−782.

(2) Betzig, E.; Patterson, G. H.; Sougrat, R.; Lindwasser, O. W.; Olenych, S.; Bonifacino, J. S.; Davidson, M. W.; Lippincott-Schwartz, J.; Hess, H. F. Imaging intracellular fluorescent proteins at nanometer resolution. *Science* **2006**, *313*, 1642−1645.

(3) Rust, M. J.; Bates, M.; Zhuang, X. Sub-diffraction-limit imaging by stochastic optical reconstruction microscopy (STORM). *Nat. Methods* **2006**, *3*, 793−795.

(4) Gahlmann, A.; Moerner, W. E. Exploring bacterial cell biology with single-molecule tracking and super-resolution imaging. *Nat. Rev. Microbiol.* **2013**, *12*, 9−22.

(5) Evans, C. L.; Xie, X. S. Coherent Anti-Stokes Raman Scattering Microscopy: Chemical Imaging for Biology and Medicine. *Annu. Rev. Anal. Chem.* **2008**, *1*, 883−909.

(6) Evans, C. L.; Potma, E. O.; Puoris'haag, M.; Cote, D.; Lin, C. P.; Xie, X. S. Chemical imaging of tissue in vivo with video-rate coherent anti-Stokes Raman scattering microscopy. *Proc. Natl. Acad. Sci. U. S. A.* **2005**, *102*, 16807−16812.

(7) Freudiger, C. W.; Min, W.; Saar, B. G.; Lu, S.; Holtom, G. R.; He, C.; Tsai, J. C.; Kang, J. X.; Xie, X. S. Label-Free Biomedical Imaging with High Sensitivity by Stimulated Raman Scattering Microscopy. *Science* **2008**, *322*, 1857−1861.

(8) Saar, B. G.; Freudiger, C. W.; Reichman, J.; Stanley, C. M.; Holtom, G. R.; Xie, X. S. Video-Rate Molecular Imaging in Vivo with Stimulated Raman Scattering. *Science* **2010**, *330*, 1368−1370.

(9) Wei, L.; Yu, Y.; Shen, Y.; Wang, M. C.; Min, W. Vibrational imaging of newly synthesized proteins in live cells by stimulated Raman scattering microscopy. *Proc. Natl. Acad. Sci. U. S. A.* **2013**, *110*, 11226−11231.

(10) Cheng, J.-X. Label-Free Spectroscopic Imaging of Lipids in Live Cells and Intact Tissues. *FASEB J.* **2013**, *27*, 813.6.

(11) Silva, W. R.; Keller, E. L.; Frontiera, R. R. Determination of Resonance Raman Cross-Sections for Use in Biological SERS Sensing with Femtosecond Stimulated Raman Spectroscopy. *Anal. Chem.* **2014**, *86*, 7782−7787.

(12) Dulkeith, E.; Morteani, A. C.; Niedereichholz, T.; Klar, T. A.; Feldmann, J.; Levi, S. A.; van Veggel, F.; Reinhoudt, D. N.; Moller, M.; Gittins, D. I. Fluorescence quenching of dye molecules near gold nanoparticles: Radiative and nonradiative effects. *Phys. Rev. Lett.* **2002**, *89*, 203002.

(13) Frontiera, R. R.; Henry, A.-I.; Gruenke, N. L.; Van Duyne, R. P. Surface-Enhanced Femtosecond Stimulated Raman Spectroscopy. *J. Phys. Chem. Lett.* **2011**, *2*, 1199−1203.

(14) Raghunathan, V.; Potma, E. O. Multiplicative and subtractive focal volume engineering in coherent Raman microscopy. *J. Opt. Soc. Am. A* **2010**, *27*, 2365−2374.

(15) Kim, H.; Bryant, G. W.; Stranick, S. J. Superresolution four-wave mixing microscopy. *Opt. Express* **2012**, *20*, 6042−6051.

(16) Wang, P.; Slipchenko, M. N.; Mitchell, J.; Yang, C.; Potma, E. O.; Xu, X.; Cheng, J.-X. Far-field imaging of non-fluorescent species with subdiffraction resolution. *Nat. Photonics* **2013**, *7*, 450−454.

DOI: 10.1021/acsphotonics.5b00467
ACS Photonics 2016, 3, 79−86

(17) Tzang, O.; Azoury, D.; Cheshnovsky, O. Super resolution methodology based on temperature dependent Raman scattering. *Opt. Express* **2015**, *23*, 17929−40.
(18) Tzang, O.; Pevzner, A.; Marvel, R. E.; Haglund, R. F.; Cheshnovsky, O. Super-Resolution in Label-Free Photomodulated Reflectivity. *Nano Lett.* **2015**, *15*, 1362−1367.
(19) Frontiera, R. R.; Mathies, R. A. Femtosecond stimulated Raman spectroscopy. *Laser Photon. Rev.* **2011**, *5*, 102−113.
(20) Harke, B.; Keller, J.; Ullal, C. K.; Westphal, V.; Schoenle, A.; Hell, S. W. Resolution scaling in STED microscopy. *Opt. Express* **2008**, *16*, 4154−4162.
(21) Willig, K. I.; Harke, B.; Medda, R.; Hell, S. W. STED microscopy with continuous wave beams. *Nat. Methods* **2007**, *4*, 915−918.
(22) Kukura, P.; McCamant, D. W.; Mathies, R. A. Femtosecond stimulated Raman spectroscopy. *Annu. Rev. Phys. Chem.* **2007**, *58*, 461−488.
(23) Ploetz, E.; Laimgruber, S.; Berner, S.; Zinth, W.; Gilch, P. Femtosecond stimulated Raman microscopy. *Appl. Phys. B: Lasers Opt.* **2007**, *87*, 389−393.
(24) Frontiera, R. R.; Shim, S.; Mathies, R. A. Origin of negative and dispersive features in anti-Stokes and resonance femtosecond stimulated Raman spectroscopy. *J. Chem. Phys.* **2008**, *129*, 064507.
(25) Naegerl, U. V.; Willig, K. I.; Hein, B.; Hell, S. W.; Bonhoeffer, T. Live-cell imaging of dendritic spines by STED microscopy. *Proc. Natl. Acad. Sci. U. S. A.* **2008**, *105*, 18982−18987.
(26) Meyer, L.; Wildanger, D.; Medda, R.; Punge, A.; Rizzoli, S. O.; Donnert, G.; Hell, S. W. Dual-color STED microscopy at 30-nm focal-plane resolution. *Small* **2008**, *4*, 1095−1100.
(27) Hein, B.; Willig, K. I.; Hell, S. W. Stimulated emission depletion (STED) nanoscopy of a fluorescent protein-labeled organelle inside a living cell. *Proc. Natl. Acad. Sci. U. S. A.* **2008**, *105*, 14271−14276.
(28) Curtin, A. E.; Skinner, R.; Sanders, A. W. A Simple Metric for Determining Resolution in Optical, Ion, and Electron Microscope Images. *Microsc. Microanal.* **2015**, *21*, 771−7.
(29) McCreery, R. L. *Raman Spectroscopy for Chemical Analysis*; John Wiley and Sons, Inc.: New York, NY, 2000.
(30) Barsi, C.; Fleischer, J. W. Nonlinear Abbe theory. *Nat. Photonics* **2013**, *7*, 639−643.
(31) Cheng, J. X.; Volkmer, A.; Xie, X. S. Theoretical and experimental characterization of coherent anti-Stokes Raman scattering microscopy. *J. Opt. Soc. Am. B* **2002**, *19*, 1363−1375.
(32) Potma, E. O.; de Boeij, W. P.; Wiersma, D. A. Nonlinear coherent four-wave mixing in optical microscopy. *J. Opt. Soc. Am. B* **2000**, *17*, 1678−1684.
(33) Zumbusch, A.; Holtom, G. R.; Xie, X. S. Three-dimensional vibrational imaging by coherent anti-Stokes Raman scattering. *Phys. Rev. Lett.* **1999**, *82*, 4142−4145.
(34) Rinia, H. A.; Burger, K. N. J.; Bonn, M.; Muller, M. Quantitative Label-Free Imaging of Lipid Composition and Packing of Individual Cellular Lipid Droplets Using Multiplex CARS Microscopy. *Biophys. J.* **2008**, *95*, 4908−4914.
(35) Slipchenko, M. N.; Chen, H.; Ely, D. R.; Jung, Y.; Carvajal, M. T.; Cheng, J.-X. Vibrational imaging of tablets by epi-detected stimulated Raman scattering microscopy. *Analyst* **2010**, *135*, 2613−2619.
(36) Offroy, M.; Moreau, M.; Sobanska, S.; Milanfar, P.; Duponchel, L. Pushing back the limits of Raman imaging by coupling super-resolution and chemometrics for aerosols characterization. *Sci. Rep.* **2015**, *5*, 12303−12303.
(37) Cleff, C.; Gross, P.; Fallnich, C.; Offerhaus, H. L.; Herek, J. L.; Kruse, K.; Beeker, W. P.; Lee, C. J.; Boller, K.-J. Stimulated-emission pumping enabling sub-diffraction-limited spatial resolution in coherent anti-Stokes Raman scattering microscopy. *Phys. Rev. A: At., Mol., Opt. Phys.* **2013**, *87*, 033830.
(38) Park, J. H.; Lee, S.-W.; Lee, E. S.; Lee, J. Y. A method for super-resolved CARS microscopy with structured illumination in two dimensions. *Opt. Express* **2014**, *22*, 9854−9870.
(39) Hajek, K. M.; Littleton, B.; Turk, D.; McIntyre, T. J.; Rubinsztein-Dunlop, H. A method for achieving super-resolved widefield CARS microscopy. *Opt. Express* **2010**, *18*, 19263−19272.

DOI: 10.1021/acsphotonics.5b00467
ACS Photonics 2016, 3, 79−86